# *Primary and metastatic intraaxial brain tumors: prospective comparison of multivoxel 2D chemical-shift imaging (CSI) proton MR spectroscopy, perfusion MRI, and histopathological findings in a group of 159 patients*

**Acta Neurochirurgica**
The European Journal of Neurosurgery

ISSN 0001-6268
Volume 153
Number 2

Acta Neurochir (2010)
153:403-412
DOI 10.1007/
s00701-010-0833-0


Springer

Acta Neurochir (2011) 153:403–412
DOI 10.1007/s00701-010-0833-0

CLINICAL ARTICLE

# Primary and metastatic intraaxial brain tumors: prospective comparison of multivoxel 2D chemical-shift imaging (CSI) proton MR spectroscopy, perfusion MRI, and histopathological findings in a group of 159 patients

**Matteo Bendini · Elisabetta Marton · Alberto Feletti · Sabrina Rossi · Stefano Curtolo · Ingrid Inches · Monica Ronzon · Pierluigi Longatti · Francesco Di Paola**

Received: 3 June 2010 / Accepted: 29 September 2010 / Published online: 17 December 2010


**Abstract**
*Background* This study aims to assess the diagnostic value of multivoxel 2D chemical-shift imaging (CSI) proton magnetic resonance (MR) spectroscopy combined with perfusion magnetic resonance imaging (MRI) in the differential diagnosis and grading of brain tumors by comparing neuroimaging data with histopathological findings obtained after resection or biopsy.
*Methods* A total of 159 patients with a previous brain tumor diagnosis underwent multivoxel 2D CSI proton MR spectroscopy and perfusion MRI. MR spectroscopy multivoxel 2D CSI was performed with an echo time of 30, TR 1,500, FOV 160 mm, acquisition time 7 min 34 s. rCBV maps were evaluated during postprocessing. Statistical analysis was performed on the examination of distributive normality, with logarithmic transformations, Fisher's test, and Bonferroni's test. We used the Pearson's test to compare percentages.
*Results* In the differential diagnosis between GBM and metastases, MR spectroscopy multivoxel 2D CSI, combined with dynamic contrast enhanced MRI (DCE-MRI) perfusion, reached high sensibility and specificity ($p<0.000001$). In brain tumor grading, the same method reached high sensibility and specificity ($p<0.000001$) in distinguishing grade III–IV gliomas but encountered difficulty in determining grades within the two main groups of primary brain tumors, especially where mixed gliomas were involved.
*Conclusions* The systematic use of CSI spectroscopy and perfusion imaging has shown a high potential in the differential diagnosis and grading of brain tumors. Further exploration into diagnostic procedures that can significantly distinguish between grade III–IV and grade II tumors is needed.

**Keywords** MRI · Spectroscopy · Perfusion · Brain tumor

M. Bendini · S. Curtolo · I. Inches · M. Ronzon · F. Di Paola
Department of Neuroradiology, Treviso Hospital,
Treviso, Italy

E. Marton · A. Feletti (✉) · P. Longatti
Department of Neurosurgery,
Treviso Hospital—University of Padova,
Piazzale Ospedale, 1,
31100 Treviso, Italy
e-mail: alberto.feletti@unipd.it

S. Rossi
Department of Pathology, Treviso Hospital,
Treviso, Italy

## Introduction

The purpose of this study was to assess the diagnostic value of multivoxel 2D CSI proton MR spectroscopy combined with perfusion MRI in the differential diagnosis of single brain lesion and grading among brain tumors, by comparing neuroimaging data with histopathological findings obtained after resection or biopsy.

Our aim was to systematically compare the accuracy of Multivoxel $^{1}$H-MR spectroscopy and perfusion MR imaging, associated with conventional contrast-enhanced anatomic MR imaging, in differentiating single metastasis and

lymphomas from glioblastoma multiforme (GBM) and, in glioma grading, by correlating morphologic, metabolic, and hemodynamic data. Our data were confirmed by histopathological findings.

## Methods

### Study design and population

We prospectively recruited 159 patients between June 2005 and February 2009. Multivoxel 2D CSI proton MR spectroscopy and perfusion MRI were systematically performed in all 159 patients, who had a previous diagnosis of brain tumor performed with CT scan. In this study, MRI was always performed after a CT scan suggestive of a "single CNS lesion". However, a CT scan does not have any element that can affect or influence the MRI reading. The presence of calcifications is the only CT scan finding that can potentially direct to a gross diagnosis of a tumor with an oligodendroglial component. Anyway, CT scan does not give elements suggestive of "mixed glioma" or of "grading". The patients comprised 88 men and 71 women (age range 17–83 years, mean age 53 years). No surgical or chemotherapy treatments had been performed prior to the study. All patients underwent major surgery or stereotactic biopsy. Glioma malignancy was graded on histological specimen as either high or low according to the World Health Organization criteria [7]. Our study comprised 135 gliomas (111 grade III–IV gliomas, 24 grade II gliomas), 12 single metastases and 12 lymphomas (NHL). The small number of metastases and lymphomas is mainly due to the fact that the study considers only single lesions, excluding all the patients with multiple lesions. All patients of this study were immunocompetent.

### MR imaging

MR imaging was performed using a Siemens Avanto 1.5 MR system with a standard head coil. Conventional MRI study was performed with conventional T2 [fast spin echo (FSE), fluid-attenuated inversion recovery (FLAIR)] and T1 sequences, with the latter being used also after the intravenous administration of paramagnetic contrast material (gadobutrol, 0.1 mmol/kg, Gadovist, Schering, Germany).

The DWI study was performed with a T2-weighted, echoplanar spin-echo sequence (TR 3,400, TE 102, matrix 192×192, slice thickness 5 mm, gap 30%) with a duration of 120 s and $b=0$, $b=500$, and $b=1{,}000$. Isotropic maps of the ADC were calculated, and the mean ADC was measured in the lesion core.

The PWI study was performed with a T2-weighted echoplanar spin-echo sequence (TR 1.480, TE 30, matrix 128×128, slice thickness 5 mm, gap 0, number of scans 50, IPAT2 Grappa 128 epi factor) with duration of 81 s. Nineteen images per second were acquired during the passage of a bolus of 0.1 mmol/kg of gadobutrol, injected with an automatic injector at a flow velocity of 5 ml/s through an 18- to 20-gauge needle cannula, followed by 20 ml of saline solution. Postprocessing was performed with a dedicated software package (Functool Siemens). Color maps of the cerebral blood volume were generated, and the mean value of the maximum regional cerebral blood volume (rCBV) was calculated by placing the region of interest in the peripheral solid areas showing the highest intensity of color. Data were then compared with those of the normal-appearing contralateral white matter and expressed as a ratio of rCBV [ratio = rCBV (lesion)/rCBV (contralateral white matter)].

MR spectroscopy multivoxel 2D CSI was performed with an echo time of 30 (TR 1,500, FOV 160 mm, acquisition time 7 min 34 s) to evaluate the levels of myoinositol (Myo), choline (Cho), creatine (Cr), *N*-acetylaspartate (NAA), and lipids. In some cases, we acquired data at intermediate TE (135) to evaluate lactate. When CSI was not possible, we performed single voxel spectroscopy 30 (SVS 30, TR 1,500 TE 30, 20×20×20 mm, 3 min 40 s) and 135 (TR 1,500 TE 30, 20×20×20 mm, 4 min 15 s) [6, 16].

The diagnoses of grade III–IV or grade II gliomas, metastasis, and lymphomas were in all cases performed by stereotactic biopsy or surgical treatment.

**Table 1** Correlation between CSI necrosis and tumor histology

| Histology | | CSI no necrosis | CSI necrosis | Row totals | *p* value |
|---|---|---|---|---|---|
| Gliomas | Count | 50 | 85 | 135 | |
| | Row percent | 37.04% | 62.96% | | 0.0003 |
| Lymphomas | Count | 0 | 12 | 12 | |
| | Row percent | 0.00% | 100.00% | | 0.0147 |
| Metastases | Count | 0 | 12 | 12 | |
| | Row percent | 0.00% | 100.00% | | 0.0147 |
| All groups | Count | 50 | 109 | 159 | |

**Table 2** Correlation between CSI necrosis and tumor grading

| Grading | | CSI no necrosis | CSI necrosis | Row totals | *p* value |
|---|---|---|---|---|---|
| II | Count | 24 | 0 | 24 | |
| | Row percent | 100.00% | 0.00% | | <0.000001 |
| III | Count | 19 | 0 | 19 | |
| | Row percent | 100.00% | 0.00% | | <0.000001 |
| IV | Count | 6 | 86 | 92 | |
| | Row percent | 6.53% | 93.47% | | <0.000001 |
| All groups | Count | 49 | 86 | 135 | |

Statistical analysis

After obtaining a series of descriptive statistics inside groups, we performed an analysis of normal distribution. When it was possible, a logarithmic transformation was performed with the purpose of normalizing the observations. If the transformation was significant, we applied an *F* ANOVA one-way Fisher's test to compare independent means, to find out the discriminative power of the dependent variable in relation with each considered parameter. To find out statistically significant differences, we used a post-hoc Bonferroni's test. For the analysis of categorical variables, a chi-squared Pearson's test was performed for percentages comparison. The significant level adopted was 0.05.

## Results

Multivoxel $^{1}$H-MR spectroscopy 2D CSI

*Necrosis*

The results are expressed in percentages. The chi-squared Pearson's test was used to compare the percentages. The significance level adopted was 0.05.

There is a statistically significant association between the dependent variable and the different histological patterns ($p$= 0.0003, 0.0147, and 0.0147 for gliomas, lymphomas, and metastases, respectively) (Table 1).

Moreover, we found out a statistically significant association between necrosis and grading of gliomas ($p<$ 0.000001) (Table 2).

*Cho/Cr*

From the descriptive statistics and from the analysis of distributive normality, we found out that distributions inside histological groups are clearly not Gaussian (Table 3). A logarithmic transformation was performed in order to normalize these distributions. We performed a classic one-way variance analysis (ANOVA). Fisher's test *F* ANOVA test was significant ($p$=0.001). Log(CSI Cho/Cr) is not discriminative among the three different histological patterns (Fig. 1).

In order to analyze the relation between Cho/Cr and glioma grades II, III, and IV, we performed a descriptive statistics with the analysis of the distributive normality (Table 4). As distributions inside groups were not Gaussian, a logarithmic transformation was performed, obtaining distributions close to normality. Therefore, we performed a classic one-way variance analysis (ANOVA). Fisher's test *F* ANOVA test was significant ($p<0.000001$) and the log (CSI Cho/Cr) resulted discriminative among the three different grading patterns (Fig. 2a). Considering the group of gliomas, the mean of log(CSI Cho/Cr) is able to clearly distinguish only glioblastoma, the values for astrocytoma, oligoastrocytoma, and oligodendroglioma being overlapped (Fig. 2b).

**Table 3** Descriptive statistics with analysis of distributive normality of CSI Cho/Cr values related to histology patterns

| Histology | CSI Cho/Cr | | | | | | | |
|---|---|---|---|---|---|---|---|---|
| | Means | Number, *N* | St. Dev. | Minimum | Maximum | Q25 | Median | Q75 |
| Gliomas | 3.763910 | 135 | 2.031946 | 1.120000 | 11.67000 | 2.100000 | 3.600000 | 5.100000 |
| Lymphomas | 2.248333 | 12 | 0.303669 | 1.600000 | 2.70000 | 2.065000 | 2.275000 | 2.450000 |
| Metastases | 1.931818 | 12 | 0.508347 | 1.400000 | 2.90000 | 1.500000 | 1.730000 | 2.320000 |
| All groups | 3.518141 | 159 | 1.973475 | 1.120000 | 11.67000 | 1.975000 | 3.365000 | 4.550000 |

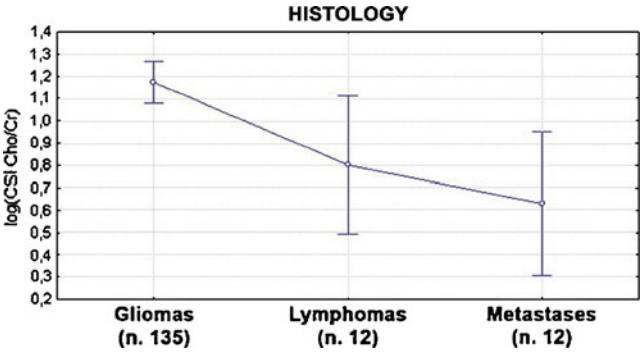


**Fig. 1** The graph shows that the log(CSI Cho/Cr) is not discriminative among gliomas, lymphomas and metastases

*Myoinositol*

Also, in this case, we performed a logarithmic transformation with a classic one-way variance analysis. Fisher's test *F* ANOVA test was significant ($p<0.000001$). The log(CSI Myo/Cr) is discriminative only for gliomas (Fig. 3a).

With the same procedures, we analyzed the relations among different glioma grades. Fisher's test *F* ANOVA was significant ($p<0.00001$) and the log(CSI Myo/Cr) was found to be significantly discriminative only for grade IV gliomas (Fig. 3b).

Finally, we analyzed the ability of distinction among gliomas. Fisher's *F* ANOVA is significant ($p<0.00001$). The log(CSI Myo/Cr) was found to be significantly reliable only to distinguish glioblastoma from the other gliomas and astrocytomas from oligodendrogliomas (Fig. 3c).

Infiltrated edema

Data were expressed in percentages of infiltration. The chi-squared Pearson's test was used to compare percentages. The significant level adopted was 0.05.

We found out a statistically significant association among the dependent variable and both the different histological patterns ($p<0.000001$) and glioma grading ($p<0.00001$) (Tables 5 and 6).

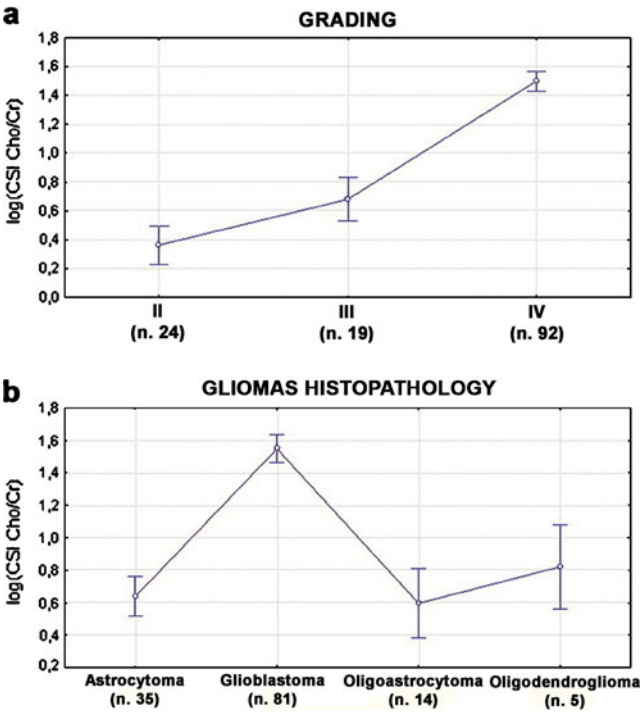


**Fig. 2** **a** The graph shows that the log(CSI Cho/Cr) is discriminative among grades II, III and IV gliomas. **b** The graph shows that the log (CSI Cho/Cr) is able to clearly distinguish only glioblastomas, but not astrocytomas, oligoastrocytomas and oligodendrogliomas

PWI

As distributions inside groups were non-normal, a logarithmic transformation was performed and a classic one-way variance analysis was used to compare independent means. Fisher's *F* ANOVA test was significant ($p<0.00001$), and the log(PWI) was found to be discriminative only for lymphomas (Fig. 4a).

With the post-hoc Bonferroni's test, the mean of log (PWI) for lymphomas (−1.801) resulted as significantly inferior ($p<0.000001$) if compared with the mean of log (PWI) for metastases (1.0501) and for gliomas (1.3406). The test was not able to discriminate among gliomas and metastases.

**Table 4** Descriptive statistics with analysis of distributive normality of CSI Cho/Cr values related to tumor grading

| Grading | CSI Cho/Cr | | | | | | | |
|---|---|---|---|---|---|---|---|---|
| | Means | Number, *N* | St. Dev. | Minimum | Maximum | Q25 | Median | Q75 |
| II | 1.491250 | 24 | 0.460730 | 1.130000 | 3.00000 | 1.200000 | 1.265000 | 1.800000 |
| III | 2.028947 | 19 | 0.467296 | 1.120000 | 2.72000 | 1.740000 | 2.100000 | 2.400000 |
| IV | 4.764719 | 92 | 1.730239 | 1.240000 | 11.67000 | 3.600000 | 4.300000 | 5.800000 |
| All groups | 3.775758 | 135 | 2.035070 | 1.120000 | 11.67000 | 2.100000 | 3.630000 | 5.100000 |

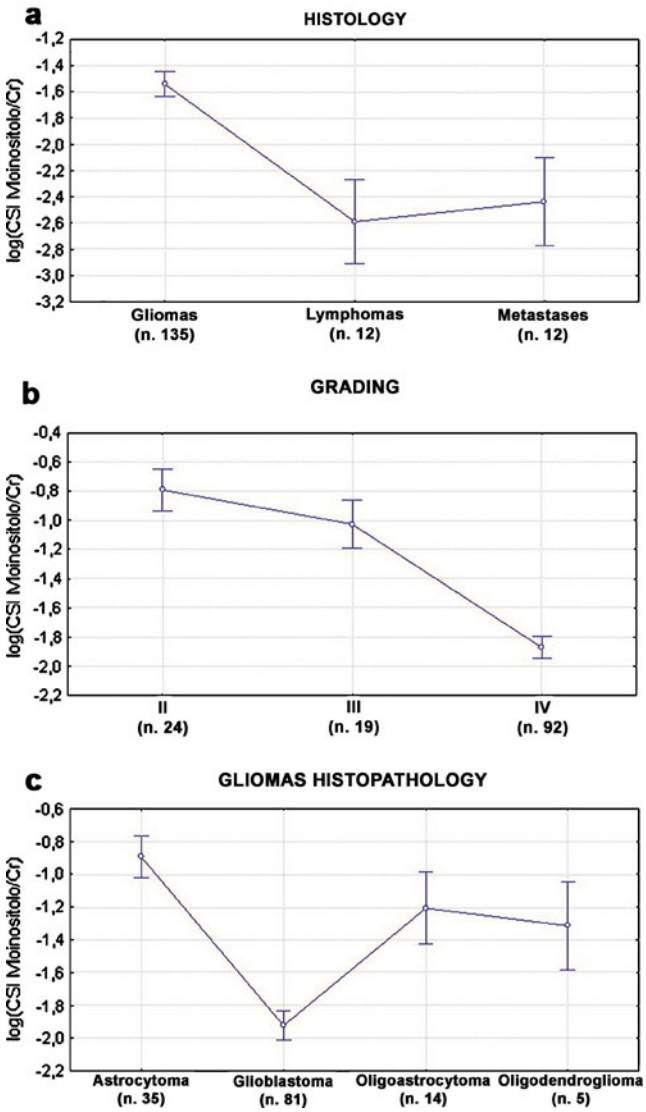


**Fig. 3** **a** The graph shows that the log(CSI Myo/Cr) is discriminative only for gliomas. **b** The graph shows that the log(CSI Myo/Cr) is significantly discriminative only for grade IV gliomas. **c** The graph shows that the log(CSI Myo/Cr) is significantly reliable only to distinguish glioblastoma from the other gliomas and astrocytomas from oligodendrogliomas

With the same method, PWI was found to be able to distinguish only grade IV gliomas ($p$=0.00001) (Fig. 4b).

The same analysis was performed for the different subtypes of gliomas. The mean value of log(PWI) was found to be significantly able to distinguish glioblastomas from other gliomas but was not reliable alone for the diagnosis of other glioma subtypes (Fig. 4c).

On the contrary, the mean value of log(PWI) was significantly capable to distinguish low-grade from high-grade gliomas ($p$=0.000001) (Fig. 4d).

## Discussion

Several published case series have reported that $^{1}$H-MR spectroscopy is very accurate in the differentiation of grade III–IV and grade II gliomas [1, 2, 8, 9, 11, 12, 19, 22, 23], using both long and/or short echo time sequences, although diagnostic accuracy is diminished in distinguishing grade III gliomas from GBM. On the other hand, Cha et al. [4] stressed that, in glioma grading, no study has compared the accuracy of $^{1}$H-MR spectroscopy with contrast-enhanced anatomic MR imaging, which should be the reference standard.

In our study, we examined brain tumor diagnosis and grading by performing a systematic study on multivoxel $^{1}$H-MR spectroscopy (CSI 30) associated with perfusion MR imaging. So far, analogous studies have been reported but performing a single-voxel $^{1}$H-MR spectroscopy [15].

In the first phase, we determined that it was important to separately analyze lactate and lipid metabolites in gliomas in order to accurately define grade III–IV gliomas. Mobile lipids are, in fact, typical of GBM owing to its pseudopalisading necrosis [14, 20]. Lactate is an end-product of nonoxidative glycolysis and is correlated with poor oxygenation levels; hypoxia promotes tumor angiogenesis. The lactate region represents areas of hypoxia but of viable tumor, while the lipid region represents areas of necrotic non-viable tissue in addition to cellular death and membrane breakdown. In standard $^{1}$H-MR spectros-

**Table 5** Correlation between infiltrated edema and tumor histology

| Histology | | CSI not infiltrated perilesional edema | CSI infiltrated perilesional edema | Row Totals | $p$ value |
|---|---|---|---|---|---|
| Gliomas | Count | 53 | 82 | 135 | |
| | Row percent | 39.26% | 60.74% | | <0.000001 |
| Lymphomas | Count | 12 | 0 | 12 | |
| | Row percent | 100.00% | 0.00% | | 0.0001 |
| Metastases | Count | 11 | 1 | 12 | |
| | Row percent | 91.66% | 8.34% | | 0.0027 |
| All groups | Count | 76 | 83 | 159 | |

**Table 6** Correlation between infiltrated edema and tumor grading

| Grading | | CSI not infiltrated perilesional edema | CSI infiltrated perilesional edema | Row totals | *p* value |
|---|---|---|---|---|---|
| II | Count | 24 | 0 | 24 | |
| | Row percent | 100.00% | 0.00% | | <0.000001 |
| III | Count | 19 | 0 | 19 | |
| | Row percent | 100.00% | 0.00% | | <0.000001 |
| IV | Count | 9 | 83 | 92 | |
| | Row percent | 9.79% | 90.21% | | <0.000001 |
| All groups | Count | 52 | 83 | 135 | |

copy acquisition (TE 30), the lactate and lipid peaks overlap within the region of 0.9 to 1.3 ppm. We used to perform CSI 30 and in some cases CSI 135 in order to define grade III–IV gliomas in our patients.

The association of $^{1}$H-MR spectroscopy with perfusion MR imaging is, however, of utmost importance [5, 17, 18, 21]. Perfusion imaging measures the degree of angiogenesis, malignancy markers, tumor progression, and infiltration. Dynamic contrast-enhanced (DCE) perfusion MR imaging is based on the "relative cerebral blood volume" (rCBV) variable, which is proportional to the area under the contrast agent concentration–time curve. Several studies have shown a strong correlation between rCBV and fibrillar astrocytoma grading: i.e., rCBV tends to increase with the grade of astrocytomas. Astrocytoma grading using rCBV is not suited to mixed gliomas or oligodendrogliomas, which may have high rCBV regardless of grade [4].

To the best of our knowledge, no studies have been published on a direct correlation between rCBV and histological features based on image-guided biopsy.

In our study, we performed a systematic analysis of perfusion MRI and correlated the neuroimaging findings with histopathological samplings obtained from both the lesion and the surrounding edematous tissue [8]. The aim was to understand the meaning of lesional and perilesional vascularization in each single histotype and the grade of

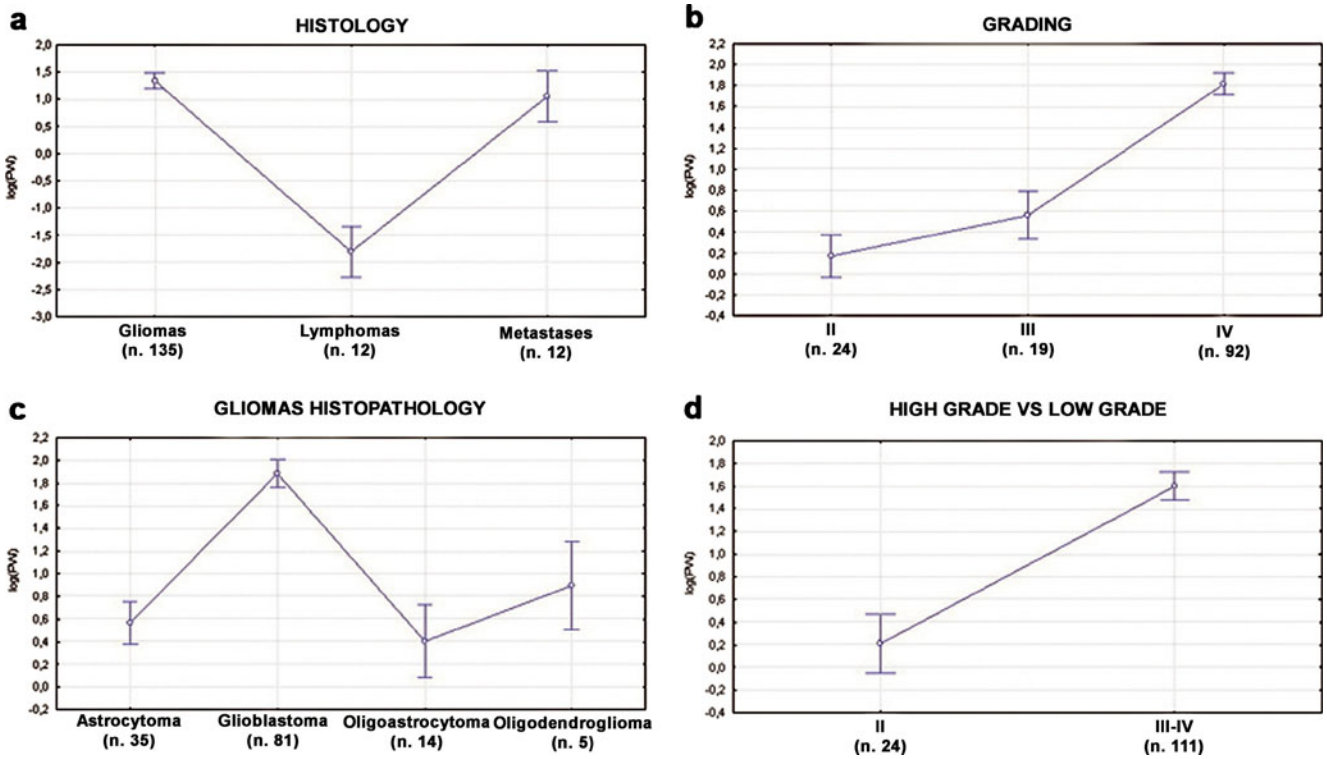


**Fig. 4** **a** The graph shows that the log(PWI) is discriminative only for lymphomas; **b** the graph shows that the log(PWI) is able to distinguish only grade IV gliomas; **c** the graph shows that the log(PWI) is able to distinguish glioblastomas from other gliomas but is not reliable alone for the diagnosis of other glioma subtypes; **d** the graph shows that the log(PWI) is significantly capable to distinguish low-grade from high-grade gliomas

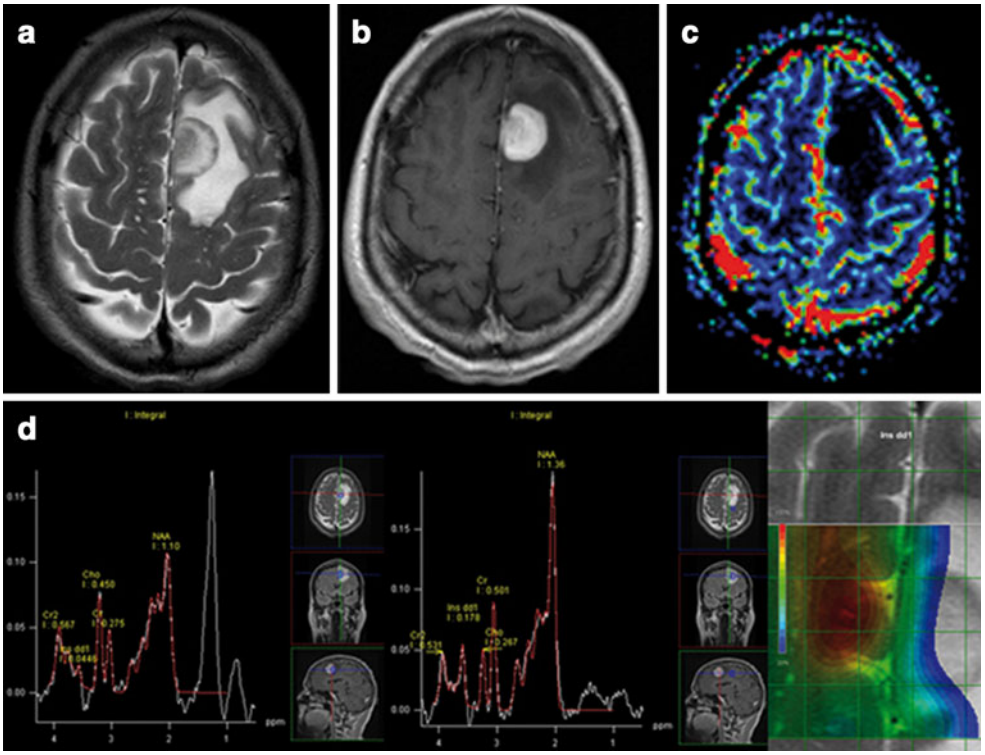


**Fig. 5** Lymphoma involving the left frontal region in a 60-year-old man; **a** T2-weighted MR shows a hypointense cellulated solid lesion, with surrounding edema; **b** contrast-enhanced T1-weighted MR shows the intense enhancement of the tumor; **c** rCBV map reveals no evidence of increased tumor vascularity; **d** multivoxel $^{1}$H-MRS (CSI with TE 30) shows the high lipid peak, relatively high choline/creatine (Cho/Cr) value, the absence of malignant tissue outside of the borders, and loss of myoinositol within the lesion

malignancy indicated by cellular infiltration of the surrounding tissue.

With the help of the BrainLab Vector Vision® system (software VectorVision cranial 7.X, iPlan cranial 2.X) or stereotaxis, the target areas of spectroscopy–perfusion MR imaging were then chosen as the target for biopsy, during resective surgery or for solely diagnostic purposes.

GBM are characterized by higher perfusion, which always presented pathological spectra due to infiltration. The combination of a high rCBV, infiltration of perilesional edema, a high Cho/Cr ratio, and a high concentration of lipids and lactate was pathognomonic and allowed us to make a correct differential diagnosis among GBM, metastases, and NHL (Fig. 5). In two cases, bleeding precluded diagnostic spectra, resulting in a wrong diagnosis. We misdiagnosed other two GBM as metastases because of a not surely infiltrating edema and a Cho/Cr ratio lower than 3.

In glioma grading, the added combination of rCBV and CSI 30 allowed us to distinguish all grade III–IV from grade II gliomas: we found a significant correlation between tumor rCBV and glioma grade, probably because the degree of vascular proliferation is an important parameter for the histopathological grading of gliomas. CSI maps were very useful in guiding biopsy primarily in huge heterogeneous lesions with different malignant parts. No grade II gliomas showed lipids or edema infiltration. Among the grade II gliomas, we were unable to differentiate the "astro" from the "oligodendro" component, but we did notice that pure oligodendrogliomas had low Myo, while LG astrocytomas always had high Myo [3].

Metastases showed very variable behaviors in rCBV and they all had a high concentration of lipids and a variable Cho/Cr ratio: the only constant parameter was the absence of infiltration of edema surrounding the lesion [13] (Fig. 6). Our only mistake was a metastasis from small cell lung cancer, with very high rCBV, since bleeding prevented us from acquiring CSI spectroscopy (Fig. 7).

In NHL, the association of low rCBV with high contrast enhancement in T1-weighted images post-contrast was pathognomonic [10]; CSI 30 resembled that of metastases: no infiltration of edema surrounding the lesion, high concentration of lipids and variable Cho/Cr ratio.

It appears that multivoxel MRS (CSI 30) can predict high-grade tumors by determining the Cho/Cr value. MRS patterns can suggest the presence of malignant tissue even outside of the enhancing borders of the lesion. A better definition of tumor margins with MRS could be useful to more precisely determine the target volume for conformational external beam radiation therapy and, therefore, to limit radiation exposure to healthy surrounding brain tissue. It could also allow the prescription of different radiation doses due to the heterogeneity of the neoplastic lesion.

The systematic use of multivoxel $^{1}$H-MR spectroscopy (CSI 30) and perfusion imaging and the possibility of comparing MR imaging results with a guided biopsy enabled us to reach differential diagnosis among GBM, metastases, and LHN with a high specificity ($p<$

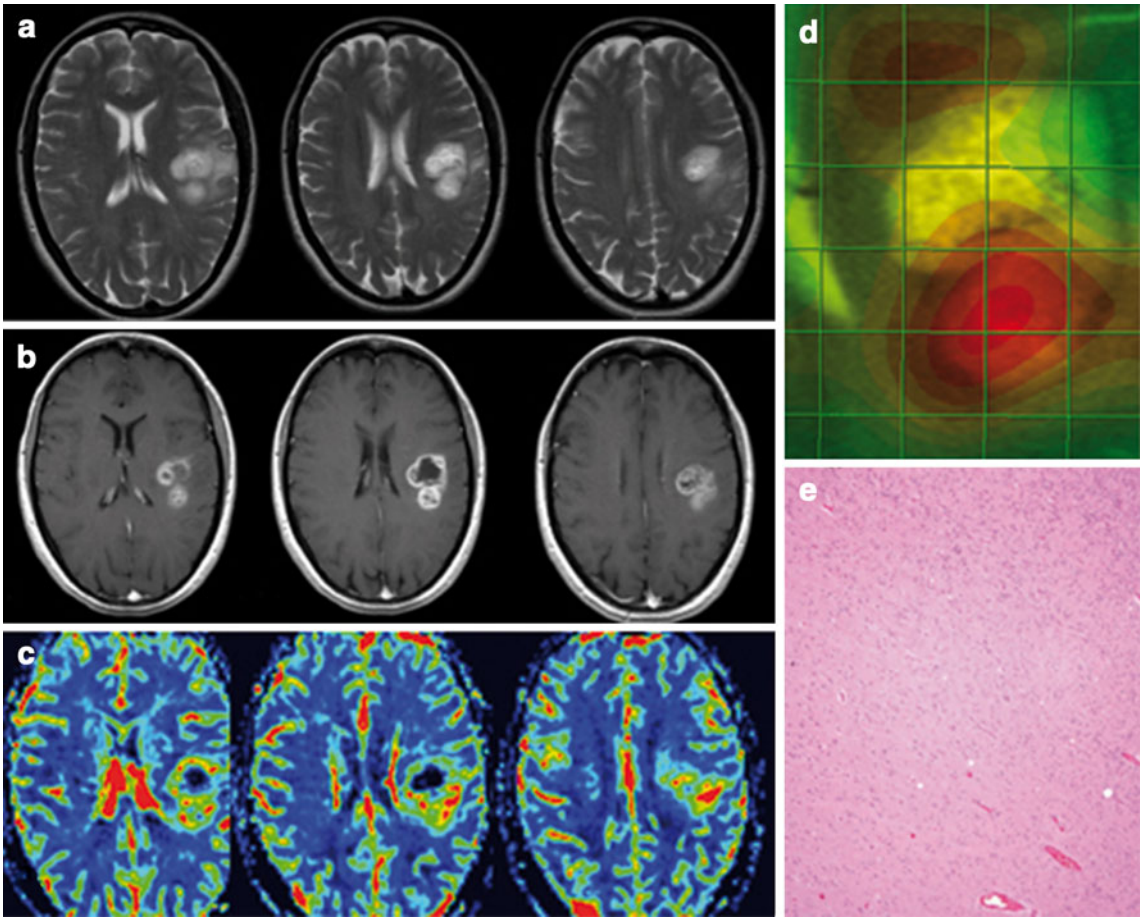


**Fig. 6** Glioblastoma in the left fronto-temporal lobe in a 55-year-old man; **a** T2-weighted MR demonstrates a mass lesion with hyperintense peritumoral edema; **b** contrast-enhanced T1-weighted MR shows the heterogeneous enhancement of the tumor; **c** rCBV map reveals a high increase in tumor vascularity; **d** multivoxel $^{1}$H-MRS (CSI with TE 30) map shows the high value of choline/creatine (Cho/Cr) in the surrounding edema, due to tumor infiltration; **e** histopathological findings show the irregular margin of the lesion compared to adjacent brain tissue (hemalum phloxine safran, ×200)

0.0000001). This analysis was also extremely useful in differential diagnosis of grading of gliomas. Further exploration is needed to find diagnostic procedures that provide significant predictive values for grading brain tumors within the two groups of grade III–IV and grade II gliomas, especially when mixed gliomas are involved. In the common clinical practice, the preoperative differential diagnosis among single CNS intraaxial tumors is not simple without tools such as MR spectroscopy and perfusion MR imaging. The presence of multiple lesions is very common, and they do not require second-level neuroimaging. The difficulty of diagnosis in the presence of single edematous lesions has always implied a histological confirmation with a stereotactic or open biopsy in order to plan the following therapies. In our clinical practice in neuro-oncology, the systematic use of MR spectroscopy and perfusion MR imaging has led to the abolishment of biopsy in the presence of a single intraaxial CNS lesion.

Patients who are eligible for surgery directly undergo major surgery, saving both time and energy and avoiding further psychological involvement. On the contrary, patients with no surgical indications (due to the general conditions and to the high surgical risk) can undergo radiotherapy and/or chemotherapy with a defined diagnosis although a real histological analysis is not available.

A biopsy is still performed in cases of CNS lymphomas after MRI diagnosis, just to obtain the typization of the tumor.

**Fig. 7** Low-grade astrocytoma in the right fronto-temporal lobe in a 30-year-old man; T2-weighted (**a**) and Flair-weighted (**b**) MR demonstrate a huge homogeneous hyperintense mass lesion with no surrounding edema; **c** contrast enhanced T1-weighted MR shows no evidence of enhancement of the tumor; **d** rCBV map reveals the absence of tumor vascularity; **e** multivoxel $^{1}$H-MRS (CSI with TE 30) map; **f** the graphic shows which part of the tumor has the highest value of choline, of choline/*N*-acetylaspartate (Cho/NAA) and of myoinositol. No evidence of lipid peak ▶

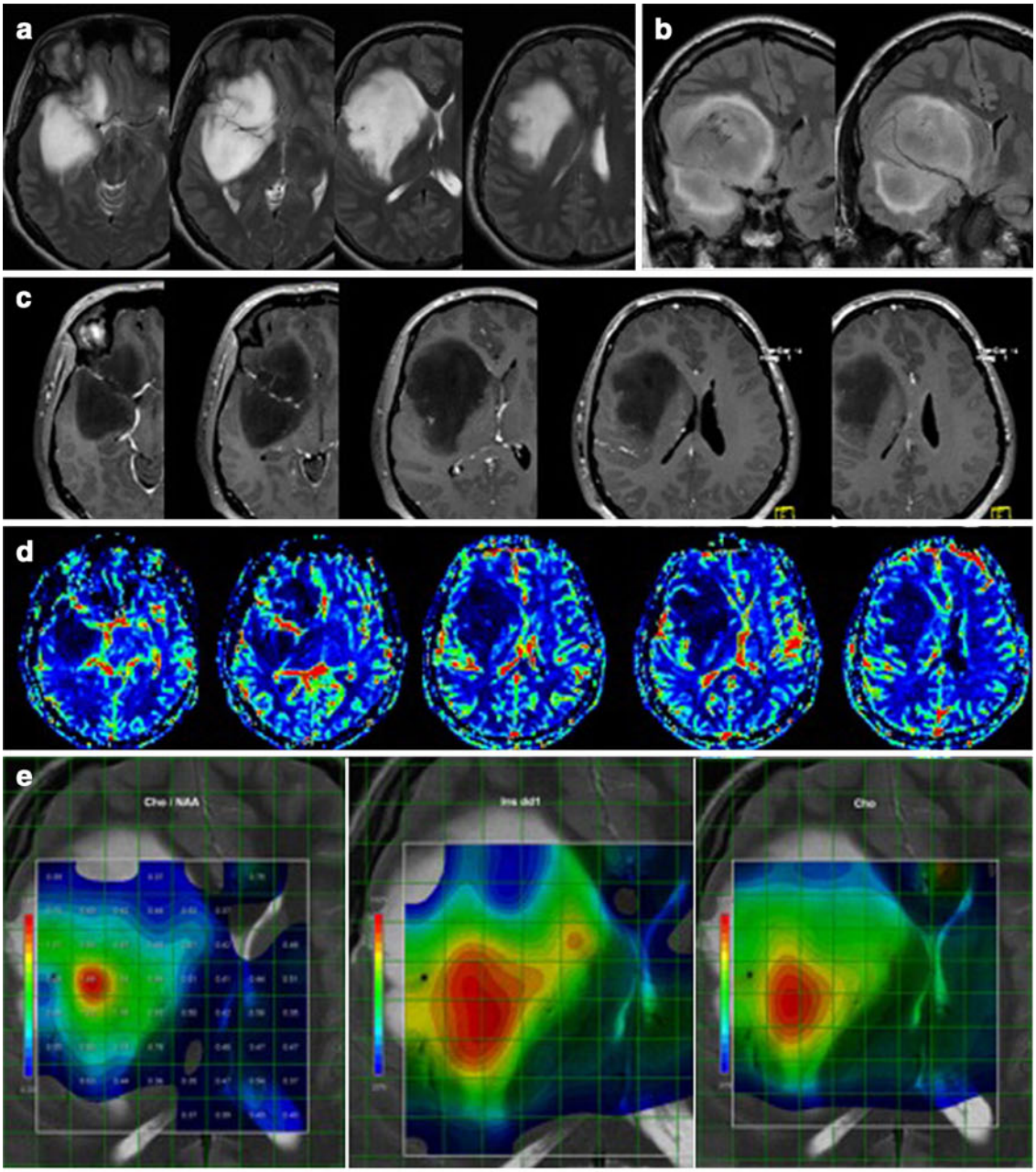


| Metabolite | Integral | Ratio |
|---|---|---|
| NAA | 0.48 | 1.58 |
| Cr | 0.31 | 1.00 |
| Cho | 0.80 | 2.63 |
| Ins dd1 | 0.31 | 1.02 |
| Cr2 | 0.69 | 2.25 |

**Ethical standards** The study has been approved by the ethics committee of the institution.

**Conflicts of interest** None.

## References


1. Burtscher IM, Skagerberg G, Geijer B, Englund E, Stahlberg F, Holtas S (2000) Proton MR spectroscopy and preoperative diagnostic accuracy: an evaluation of intracranial mass lesions characterized by stereotactic biopsy findings. Am J Neuroradiol 21:84–93
2. Castillo M, Kwock L, Mukherji SK (1996) Clinical applications of proton MR spectroscopy. Am J Neuroradiol 17:1–15
3. Castillo M, Smith JK, Kwock L (2000) Correlation of myo-inositol levels and grading of cerebral astrocytomas. Am J Neuroradiol 21:1645–1649
4. Cha S (2006) Update on brain tumor imaging: from anatomy to physiology. Am J Neuroradiol 27:806–809
5. Chiang IC, Kuo YT, Lu CY, Yeung KW, Lin WC, Sheu FO, Liu GC (2004) Distinction between high-grade gliomas and solitary metastases using peritumoral 3-T magnetic resonance spectroscopy, diffusion, and perfusion imagings. Neuroradiology 46:619–627
6. Danielsen ER, Ross B (1999) Basic physics of MRS. In: Danielsen ER, Ross B (eds) Magnetic resonance spectroscopy diagnosis of neurological diseases. New York, Marcel Dekker, pp 5–22
7. Daumas-Duport C, Beuvon F, Varlet P, Fallet-Bianco C (2000) Gliomas: WHO and Sainte-Anne Hospital classifications. Ann Pathol 20:413–428
8. Dowling C, Bollen AW, Noworolski SM, McDermott MW, Barbaro NM, Day MR, Henry RG, Chang SM, Dillon WP, Nelson SJ, Vigneron DB (2001) Preoperative proton MR spectroscopic imaging of brain tumors: correlation with histopathologic analysis of resection specimens. Am J Neuroradiol 22:604–612
9. Grand S, Kremer S, Tropres I, Pasteris C, Krainik A, Hoffmann D, Chabardes S, Berger F, Pasquier B, Lefournier V, Le Bas JF (2006) Perfusion–diffusion $^{1}$H spectroscopy: role in the diagnosis and follow-up of supratentorial brain tumours in adults. Rev Neurol (Paris) 162:1204–1220
10. Hartmann M, Heiland S, Harting I, Tronnier VM, Sommer C, Ludwig R, Sartor K (2003) Distinguishing of primary cerebral lymphoma from high-grade glioma with perfusion-weighted magnetic resonance imaging. Neurosci Lett 338:119–122
11. Hollingworth W, Medina LS, Lenkinski RE, Shibata DK, Bernal B, Zurakowski D, Comstock B, Jarvik JG (2006) A systematic literature review of magnetic resonance spectroscopy for the characterization of brain tumors. Am J Neuroradiol 27:1404–1411
12. Howe FA, Barton SJ, Cudlip SA, Stubbs M, Saunders DE, Murphy M, Wilkins P, Opstad KS, Doyle VL, McLean MA, Bell BA, Griffiths JR (2003) Metabolic profiles of human brain tumors using quantitative in vivo $^{1}$H magnetic resonance spectroscopy. Magn Reson Med 49:223–232
13. Ishimaru H, Morikawa M, Iwanaga S, Kaminogo M, Ochi M, Hayashi K (2001) Differentiation between high-grade glioma and metastatic brain tumor using single-voxel proton MR spectroscopy. Eur Radiol 11:1784–1791
14. Kaminogo M, Ishimaru H, Morikawa M, Ochi M, Ushijima R, Tani M, Matsuo Y, Kawakubo J, Shibata S (2001) Diagnostic potential of short echo time MR spectroscopy of gliomas with single-voxel and point-resolved spatially localised proton spectroscopy of brain. Neuroradiology 43:353–363
15. Kim JH, Chang KH, Na DG, Song IC, Kwon BJ, Han MH, Kim K (2006) 3T $^{1}$H-MR spectroscopy in grading of cerebral gliomas: comparison of short and intermediate echo time sequences. Am J Neuroradiol 27:1412–1418
16. Kwock L (1998) Localized MR spectroscopy: basic principles. Neuroimaging Clin N Am 8:713–731
17. Law M, Cha S, Knopp EA, Johnson G, Arnett J, Litt AW (2002) High-grade gliomas and solitary metastases: differentiation by using perfusion and proton spectroscopic MR imaging. Radiology 222:715–721
18. Law M, Yang S, Babb JS, Knopp EA, Golfinos JG, Zagzag D, Johnson G (2004) Comparison of cerebral blood volume and vascular permeability from dynamic susceptibility contrast-enhanced perfusion MR imaging with glioma grade. Am J Neuroradiol 25:746–755
19. Majós C, Alonso J, Aguilera C, Serrallonga M, Pérez-Martín J, Acebes JJ, Arùs C, Gili J (2003) Proton magnetic resonance spectroscopy ((1)H MRS) of human brain tumours: assessment of differences between tumour types and its applicability in brain tumour categorization. Eur Radiol 13:582–591
20. Majós C, Julià-Sapé M, Alonso J, Serrallonga M, Aguilera C, Acebes JJ, Arùs C, Gili J (2004) Brain tumor classification by proton MR spectroscopy: comparison of diagnostic accuracy at short and long TE. Am J Neuroradiol 25:1696–1704
21. Rollin N, Guyotat J, Streichenberger N, Honnorat J, Tran Minh VA, Cotton F (2006) Clinical relevance of diffusion and perfusion magnetic resonance imaging in assessing intra-axial brain tumors. Neuroradiology 48:150–159
22. Sibtain NA, Howe FA, Saunders DE (2007) The clinical value of proton magnetic resonance spectroscopy in adult brain tumours. Clin Radiol 62:109–119
23. Tate AR, Majós C, Moreno A, Howe FA, Griffiths JR, Arùs C (2003) Automated classification of short echo time in vivo $^{1}$H brain tumor spectra: a multicenter study. Magn Reson Med 49:29–36